JOURNAL OF THE ROYAL SOCIETY Interface
FirstCite® e-publishing

J. R. Soc. Interface
doi:10.1098/rsif.2006.0151
Published online

Nonlinear mechanics of soft fibrous networks

A. Kabla[1] and L. Mahadevan[1,2,*]

[1]*Division of Engineering and Applied Sciences, Harvard University, Cambridge, MA 02138, USA*
[2]*Department of Systems Biology, Harvard Medical School, Boston, MA 02115, USA*

Mechanical networks of fibres arise on a range of scales in nature and technology, from the cytoskeleton of a cell to blood clots, from textiles and felts to skin and collageneous tissues. Their collective response is dependent on the individual response of the constituent filaments as well as density, topology and order in the network. Here, we use the example of a low-density synthetic felt of athermal filaments to study the generic features of the mechanical response of such networks including strain stiffening and large effective Poisson ratios. A simple microscopic model allows us to explain these features of our observations, and provides us with a baseline framework to understand active biomechanical networks.

Keywords: nonlinear mechanics; fibre network; biomaterials

1. INTRODUCTION

Fibre networks are versatile functional materials with tunable mechanical properties. They have a high specific stiffness (stiffness/density) which can be controlled by variations in local density, connectivity and ordering. Networks of thermal and athermal fibres arise naturally on a range of length-scales from the nanometre scale in the cytoskeleton of a cell (Alberts *et al.* 2002), blood clots (Janmey *et al.* 1983; Weisel 2004) or biological tissues (Sacks 2000; Layton & Sastry 2004) to the millimetre scale in felts and fibrous mats (Hearle *et al.* 1969; Chawla 1998; Lee *et al.* 2005). To understand the generic properties of such networks, we need to distinguish the effects of molecular, kinetic and hydrodynamic processes from those that arise purely from geometry and connectivity. At the fibre scale, individual filaments are always softer in bending than in stretching, a fact that is due more to geometry than material properties (Love 1944). When internal energy scales are comparable to thermal energy in semi-flexible polymers for instance, the balance between entropic and enthalpic effects (MacKintosh *et al.* 1995; Marko & Siggia 1995) leads to the appearance of wrinkles; the free-energy cost associated with ironing out these forms the basis for the elasticity of such filaments. When internal energy scales are large compared with thermal energy, the origins of elasticity are qualitatively different and arise from purely enthalpic effects owing to bending, unbending and stretching of individual filaments. Despite this qualitative difference between thermal and athermal filaments, the topological constraints associated with crosslinks and the disorder inherent in the connectivity of the network (Ryan *et al.* 1999) are common to all mechanical networks.

*Author for correspondence (lm@deas.harvard.edu).

In these systems, a natural question is the origin of the striking nonlinear mechanical behaviour observed in biaxial tests (Sacks 2000; Roeder *et al.* 2004*a*) and rheological measurements (Gardel *et al.* 2004; Storm *et al.* 2005). Two independent causes are (i) the nonlinear mechanical response of a single fibre and (ii) the non-affine collective deformation of the network. Recent experimental and theoretical studies of microscopic polymer networks (Gardel *et al.* 2004; Storm *et al.* 2005) ascribe the nonlinear network response directly to the nonlinearities of individual fibres. However, numerical simulations (Head *et al.* 2003; Onck *et al.* 2005; Chandran & Barocas 2006; Heussinger & Frey 2006) of mechanical networks suggest that strain stiffening could also arise owing to non-affine deformations, which are highly dependent on the network connectivity and organization. To disentangle the relative contributions of these effects, we need to characterize and couple the microscopic mechanics to the network behaviour. In this paper, we study a synthetic macroscopic fibrous network and show that the single fibre response suffices to explain the main observations both qualitatively and quantitatively.

2. MATERIAL CHARACTERIZATION

We performed uniaxial tests on a synthetic felt (Air-Lite, polyester quilt batting) composed of entangled polyester filaments of typical lengths ranging from 4 to 10 cm and diameter 30 to 50 μm. The felt has a low density, close to 1.5×10^{-2} g cm^{-2}. Individual filaments can be removed easily and interact with each other only frictionally; there are no topological knots or adhesion between fibres. The felt is quasi-two-dimensional, i.e. it is made up of layers which are much thinner (approx. 2 mm) than the length of individual fibres; however, in each layer, the fibres are

Received 22 June 2006
Accepted 25 July 2006

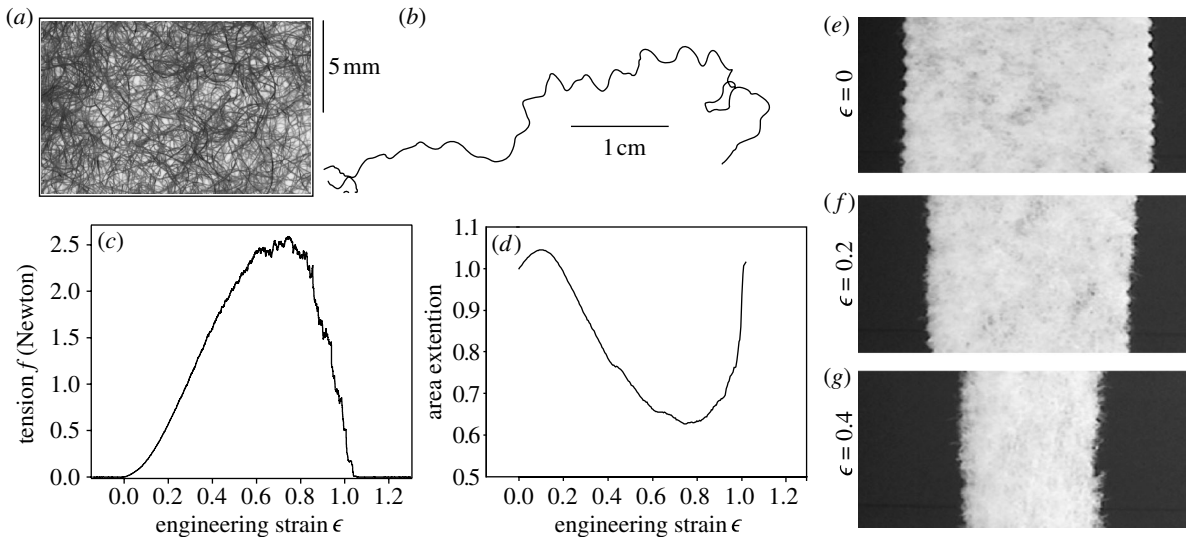

Figure 1. Structure and response of a soft mechanical network. (*a*) Typical piece of felt. (*b*) A single polyester fibre (length 7 cm, diameter 30 µm). (*c*) Response to a uniform strain rate ($\dot{\epsilon} = 4.3 \times 10^{-3}\ \mathrm{s}^{-1}$) showing tension versus strain curve. (*d*) Areal response $A(\epsilon)/A(0)$ versus strain ϵ. The increase in the area observed as the felt breaks is due to the felt relaxing back to its initial area as the global tensile stress goes back to zero. (*e–g*) Width of the felt strip for various imposed strains.

strongly entangled and completely disordered (figure 1*a*). We probe the tensile behaviour of a strip of felt, with dimension of 23×7.5 cm, clamped at one end to a motorized translation stage (Stage Newport IMS500 and Controller Newport ESP300) and to a force sensor at the other (Futek LSB200 100*g* or 1 lb). The net force exerted on the sensor, noted *f*, is recorded as the material is stretched. A large sampling rate (1 kHz) and a Gaussian filter are used to remove residual acquisition noise, leading to a precision on the force measurements of the order of 10^{-4} N. A charge-coupled device (CCD) camera is used to simultaneously record the shape of the material, change in the projected area and average thickness of the strip.

Here we focus on the quasistatic response, where the typical deformation rate is much smaller than the network reorganization rate and the force per fibre is small enough to neglect individual fibre creep. To ensure this, we pull on the felt at a speed 1 mm s^{-1}, corresponding to a stain rate of around $4 \times 10^{-3}\ \mathrm{s}^{-1}$. In figure 1*c*, we show the complete force–extension curve until the felt breaks. As the felt is stretched, the stiffness increases monotonically before the material yields and eventually fails. Simultaneously, the planar area of the strip of felt changes. For small deformations, the area $A(\epsilon)$ increases but once the longitudinal strain exceeds 0.1, the area decreases substantially, so that the incremental Poisson ratio $\nu = 1 - (1/A(0))\partial A/\partial\epsilon$ is greater than unity[1] (the strip thickness remains roughly constant until just before the felt fails). These constitutive behaviours of the felt are in stark contrast with that of elastomeric materials such as rubber (Treloar 1972) which are incompressible ($\nu = 1/2$) and whose stiffness is non-monotonic with strain. Instead, the felt shows similarities with biological tissues (Blatz 1969; Vincent 1990; Shadwick 1999), skin, blood clots (Janmey *et al.* 1983; Weisel 2004), hair, hagfish slime (Fudge *et al.* 2003), spider silk (Becker *et al.* 2003), single cells (Fernandez *et al.* in press) and *in vitro* models for the cytoskeleton (Gardel *et al.* 2004).

3. SINGLE FIBRE MECHANICS

3.1. Experiments

Understanding this behaviour requires the characterization of the geometry and mechanical response of the individual fibres in the felt; the latter has a natural distribution of athermal bends which are pulled taut as the material is stretched. The fibre geometry is characterized by the statistics of its quenched curvature, which we extract by analysing the natural unstrained profile of a few fibres that are gently confined[2] between a glass plate and a dark background and scanned digitally at a resolution of 600 dots per inch. This allows us to compute the spatial spectrum of the curvature (figure 2*a*)— we see that although there is a peak, the spectrum involves lengthscales from 0.7 mm up to the natural length of the fibre.

The mechanical response of such a naturally curved fibre is dominated by the unbending of the curved regions; as the applied force is increased, first the longer wavelengths are ironed out, followed by the shorter ones, until the entire fibre is geometrically straightened. Only then will the fibre be physically stretched. In figure 2*b*—we see that we show the measured force–extension curve for an individual fibre. Denoting the fibre end-to-end distance scaled by its contour

[1]In a displacement-controlled experiment, the force decreases just before the failure. Since the felt recovers most of its initial volume, except where the material has failed, the increase in the surface area of the sample seen in figure 1*d* is essentially an elastic effect.

[2]Although the fibre follows a tortuous path in space and thus has a non-zero geometric torsion, the measured torsion is small relative to the curvature so that a projected image provides a fairly accurate description of the curvature of the fibre over most wavelengths. However, on length-scales that are comparable to the fibre length, this description breaks down owing to large fluctuations from one fibre to another.

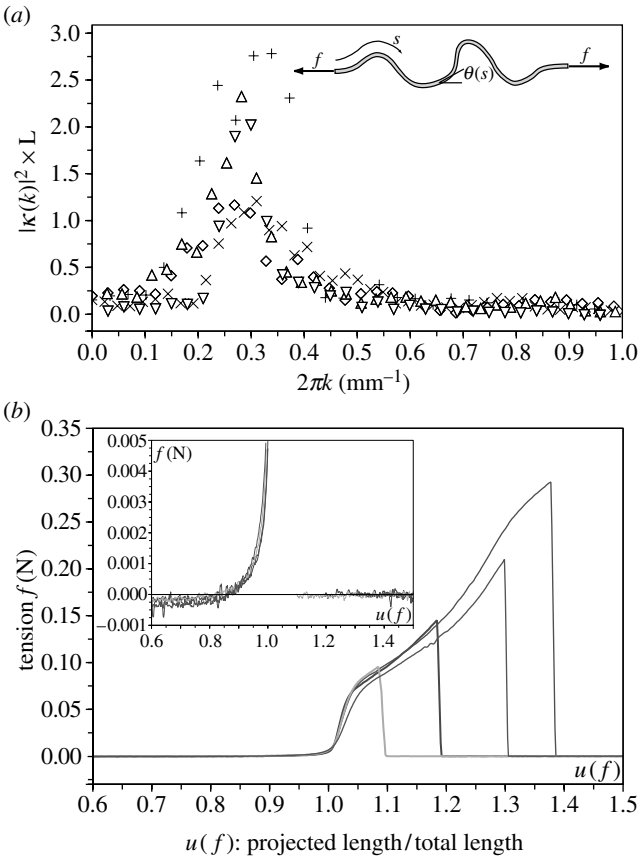

Figure 2. Single fiber characterization. (*a*) Spatial power spectrum of the fibre curvature showing the squared Fourier amplitudes as a function of the wave number k, presented for five different fibres. L represents the total length for each individual fibre. Inset: schematic of an individual fibre showing the notation used. (*b*) Force–extension relationship for four single fibres. The inset details the low-force regime. The knee characterizes the onset of plasticity.

length as $u(f)$, where f is the applied force, we can identify three regimes: $u<1$, $1<u\leq 1.05$ and $u>1.05$. When $u>1.05$, the fibre deforms irreversibly before breaking. When $1<u\leq 1.05$, the fibre stretches elastically with a Young's modulus of 2.5 GPa. The quenched curvature determines the fibre mechanical response for $u<1$, the case of most interest here. In the inset to figure 2*b*, we zoom in on this regime and see that for a typical fibre $u(0)\approx 0.85$. For small tensile strains, i.e. $u(0)<u\leq 1$, the fibre shows a strong stiffening behaviour. For small compressive strains, i.e. $u<u(0)$, the fibre buckles, thus limiting its ability to sustain any load.

3.2. Model

The microscopic behaviour of the fibre is described by the theory of the Elastica (Love 1944) for the geometrically nonlinear deformations of a slender filament with a non-zero natural curvature. The force–extension relationship of a naturally curved rod is in general hard to obtain analytically. On stretching, the rod bends and twists, and the response depends strongly on the initial geometry. For simplicity, we consider the planar deformations of an elastic rod with a natural inhomogeneous curvature $\kappa_0(s)$ where s is the arc-length along the fibre (assumed to be inextensible). The rod is clamped at both ends, and a force $\vec{f}$ is applied along the end-to-end direction. Force balance along the rod leads to $\partial_s \vec{f} = 0$; the force is constant in magnitude and orientation, while torque balance gives

$$f \sin\theta + \partial_s M = 0, \tag{3.1}$$

where $\theta(s)$ is defined as the angle between the force and the local tangent to the rod, f is the magnitude of the force and M is the torque. Assuming that the deformations are of long wavelength type, the local torque is related to the local curvature by $M = -B\cdot(\kappa(s)-\kappa_0(s))$, where κ_0 and κ are, respectively, the natural and the actual curvature of the fibre and B its bending stiffness. Combining the latter with equation (3.1) leads to

$$B\partial_s(\partial_s\theta - \kappa_0(s)) - f\sin\theta = 0. \tag{3.2}$$

To complete the formulation of the problem, we assume clamped and periodic boundary conditions ($\theta(0)=\theta(L)$ and $M(0)=M(L)$), consistent with the load being oriented along the line joining the clamped ends. In terms of $\theta(s)$, we can then determine the force–extension relation using the kinematic relation

$$u(f) = \frac{1}{L}\int_0^L \cos\theta \, \mathrm{d}s. \tag{3.3}$$

We used the software Scilab[3] to solve equations (3.2) and (3.3). Figure 3 shows the force–extension curves of three fibres with different naturally curved shapes, characterized by amplitude A_k and wavelength $2\pi/k$, given by $\kappa_0 = A_k\cdot\cos(ks+\phi)$, with $k=2\pi n/L$, $n\in\mathbb{N}$. If the fibre is weakly curved, we may use a linearized version of equation (3.2) whose solution yields

$$\theta(s,f) = \frac{\partial_s\kappa_0(s)}{(f/B)+k^2}. \tag{3.4}$$

In figure 3*a*, we show the force–extension curves obtained with equations (3.3)–(3.4) and see that the linear estimate is in good agreement with the numerical solution of equations (3.2)–(3.3) for weakly curved fibres. Experimentally, since $u(0)\approx 0.85$, we find that the linearized theory is sufficient to describe the force–extension curves. An alternative multi-scale approach for the fibre response is presented in appendix A.

Using the measured curvature spectrum of an individual fibre expressed as $\kappa_0 = \sum_k A_k\cdot\cos(ks+\phi_k)$, we solve equations (3.2) and (3.3) numerically to get the force–extension curve shown in figure 2*b*, showing good agreement with the experimentally measured curve with a single physical parameter, the bending stiffness B. In particular, we see that the experimentally observed stiffening of the filament in the nonlinearly elastic regime corresponds to the ironing out of the quenched curvature. To understand this qualitatively, it is sufficient to analyse equations (3.2) and (3.3) in the asymptotic limit $\theta \ll 1$, which yields an approximate expression for the scaled end-to-end distance $u(f)$,

$$u(f) \approx 1 - \sum_k \frac{A_k^2 k^2}{4\left(\frac{f}{B}+k^2\right)^2}. \tag{3.5}$$

Thus, while the response is linear for small tensile strains, softer (larger length-scale) modes are progressively

[3]Scilab: www.scilab.org/

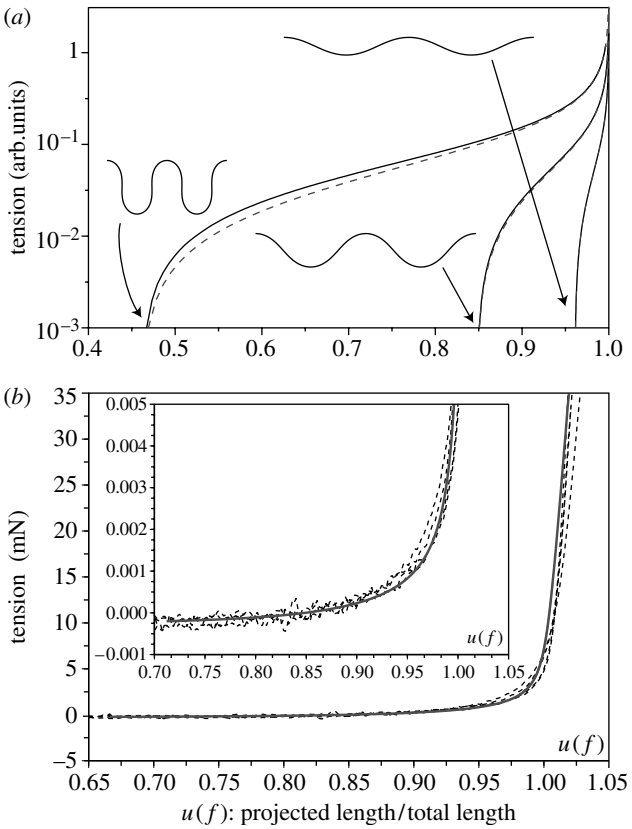

Figure 3. (*a*) Force–displacement curves for various natural geometries: solid lines correspond to numerical integration and the dashed line to the analytical solution of the linear model (3.3)–(3.4). From right to left, $\kappa_0 = 2.5\cos(2\pi s)$, $\kappa_0 = 5\cos(2\pi s)$ and $\kappa_0 = 10\cos(2\pi s)$. (*b*) Extension response of a curved fibre (solid line) obtained numerically by solving (3.2)–(3.3) given the measured average power spectrum. The only parameter required to fit the experimental data shown in dashed lines is the bending stiffness ($B \approx 2\times10^{-10}$ Jm). Inset details the low-force regime.

ironed out, until the force diverges as $f \approx 1/\sqrt{(1-u)}$ when the fibre is stretched to its natural length. This divergence is tempered in practice by a finite stretching stiffness of the fibre. This microscopic picture for strain stiffening as a consequence of quenched curvature in an athermal fibre is qualitatively similar to the experimentally observed (Cluzel *et al.* 1996; Smith *et al.* 1996) and theoretically predicted (MacKintosh *et al.* 1995; Marko & Siggia 1995) behaviour of a semi-flexible polymer though the underlying mechanisms are quantitatively different.

4. MACROSCOPIC RESPONSE

4.1. Elastic and plastic response

When moving from the above microscopic description of fibre behaviour to the collective behaviour of the network, we must first identify the reversible elastic and the irreversible plastic contributions in the macroscopic response of the felt shown in figure 1*c*,*d*. A natural way to address this question is to impose cyclic strains of gradually increasing amplitudes and measure the response of the network. In figure 4*a*, we show that the force–displacement response in such an experiment has two distinct regimes. For strains smaller than the maximum strain on a previous cycle, the unloading (solid) and loading (dashed) curves are fairly close; in figure 4*a*, an example of this is shown in the path 1–2 which encloses a loop defining what we call weak hysteresis. When the strain is increased beyond the maximum seen on a previous cycle (labelled 3 in figure 4*a*), the response curve is qualitatively different; the envelope of these curves is coincident with the response to monotonic loading shown in figure 1. When combined with a typical unloading cycle, the resulting loop is much larger and defines what we call strong hysteresis.

Irreversibility in these networks arises from three basic causes: (i) fibre–fibre frictional interactions, which are responsible for the weak hysteresis in a single unloading–reloading cycle; (ii) collective rearrangements; in the fibre network which occur when fibres disentangle during loading along the envelope curve associated with a monotonically increasing displacement; and (iii) individual fibre creep, which is negligible for the force range we consider as we will show later. For a reasonable approximation, the reversible elastic response is given by the unloading curves noted $\epsilon_i(f)$ and shown as solid lines in figure 4*a*[4]. As a result of network reorganization, the force vanishes after each cycle for a strain $\epsilon_i(0) > 0$. A semi-log representation of the curves provides an unambiguous way to estimate this strain (inset to figure 4*b*) whose dependence with the maximal imposed strain is plotted in the inset to figure 4*c*. We use this reference state to scale the applied strain and the area of the felt for each unloading curve and define the corrected strain and area as

$$\epsilon_{i,c}(f) = \frac{\epsilon_i(f) - \epsilon_i(0)}{1 + \epsilon_i(0)} \text{ and } a_{i,c}(f) = \frac{a_i(f)}{a_i(0)}. \qquad (4.1)$$

In figure 4*b*,*c*, we show the tension and the corrected area $a_{i,c}$ as a function of the corrected strain $\epsilon_{i,c}$. For any given curve, as the elastic strain increases, the felt stiffens strongly and its incremental Poisson ratio $\nu_i = 1 - \partial a_{i,c}/\partial \epsilon_{i,c}$ increases and eventually exceeds unity. In particular, the progressive network reorganization that occurs with the increase in the cycle amplitude of the strain leads to a progressive softening of the mechanical response and a reinforcement of the Poisson effect. A model for the mechanical response of the network requires quantification of (i) the mechanical response of individual fibres and (ii) the local connectivity, geometry and frustrated internal stress in the network, some of which are history dependent. We will consider this next.

4.2. Network model

Starting with the microscopic response of a fibre (figure 3*b*), we assume a unit cell with a minimal network connectivity (figure 4*d*) inspired by similar models in polymer physics (Flory 1959). To parametrize the individual fibres in this network, we prescribe

[4]Repeated cycles of loading and unloading up to the same amplitude show that the unloading curve is highly reproducible while the loading curve fluctuates significantly. We thus use the unloading curves to characterize the elastic response for a given state of the network which itself evolves as a function of the maximum strain.

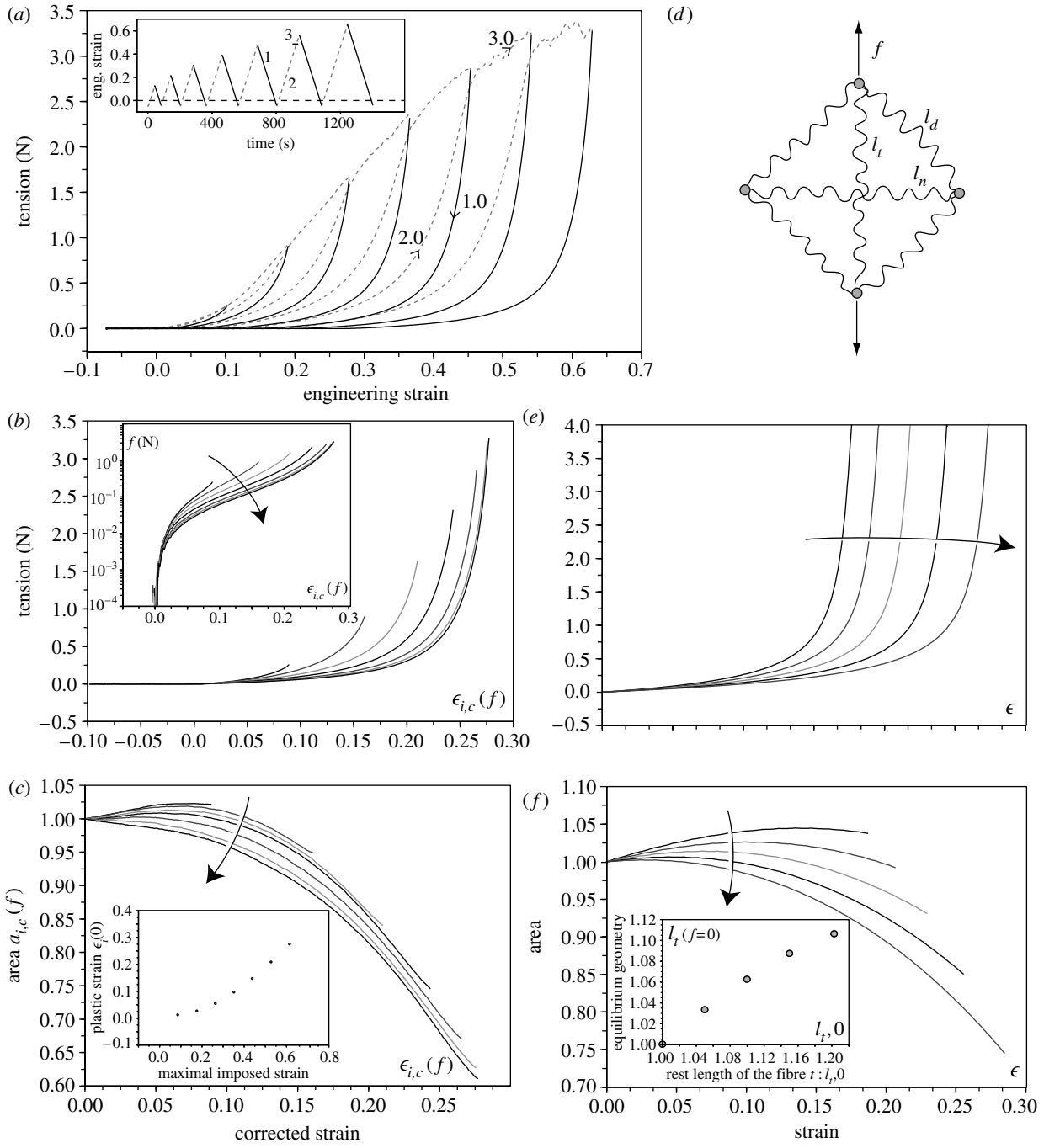

Figure 4. Elastic response of the network. (*a*) Response of the felt strip to strain cycles of growing amplitude. Inset shows the time evolution of the imposed strain. The strain rate is $4.3\times10^{-3}\,\mathrm{s}^{-1}$. In a cycle, the dashed curves correspond to the increase in strain and solid curves to the decrease in strain; the latter corresponds to the elastic strain. (*b*) Tension corrected elastic strain and (*c*) corrected area as a function of the corrected strain (see text). Inset: measured residual plastic strain $\epsilon_i(0)$ and maximal imposed strain for each cycle *i*. (*d*) Minimal network of fibres and its deformation due to an applied force. Results of the network model for the evolution of (*e*) the tension and (*f*) the network area as a function of the applied strain, for five different fibres. Inset: the plasticity parameter $l_{t,0}$ in the network model and its effect on the load-free equilibrated geometry. Forces have been multiplied by 350 in order to match the experimental values; this corresponds roughly to the number of stretched fibres in a section of the strip of felt.

all their force-free (rest) lengths, denoted $l_{t,0}$, $l_{n,0}$ and $l_{d,0}$ for the fibres tangential, normal and at 45° to the load, respectively. The initial state is defined by $l_{t,0} = l_{n,0} = \sqrt{2}l_{d,0}$, when the network is initially under zero applied load. To determine both the purely elastic force–extension curve and the incremental Poisson ratio, we calculate the equilibrium configuration of the unit cell as a function of the applied force.

In the physical system, the load is expected to disentangle the fibres along the direction of its application causing network reorganization. Once such a fibre is disentangled, the network is likely to recruit the next shortest available fibre in the same direction to sustain the applied load. We model this by increasing the rest length $l_{t,0}$ of this fibre, which results in a residually strained network; an increase in $l_{t,0}$

results in an elongation of the equilibrated network in the load direction ($l_\alpha(f{=}0) \neq l_{\alpha,0}$) as described in the inset to figure 4*f*. In order to identify the dependence of the plasticity parameter $l_{t,0}$ on the global elastic response, we scale the measured strain and the area relative to that of the force-free equilibrated configuration defining

$$\epsilon(f) = \frac{l_t(f) - l_t(0)}{l_t(0)} \text{ and } \quad a(f) = \frac{l_n(f) \cdot l_t(f)}{l_n(0) \cdot l_t(0)}, \qquad (4.2)$$

where $l_t(f)$ and $l_n(f)$ are the equilibrated length of the fibres oriented along and normal to the loading direction, respectively. Calculating the constitutive response as a function of this simple parametrization of network reorganization leads to the sequence of curves in figure 4*e*,*f*, and compares very well with the experimental data in figure 4*b*,*c*. The qualitative trends seen herein are independent of the details of network connectivity as long as the nodal coordination number satisfies Maxwell's rigidity criterion (Maxwell 1864). Quantitatively, the total measured force is about 350 times the force on a unit cell, a number which corresponds to the typical number of stretched fibres in the direction of the load. Based on the observed material density, the number of fibres initially oriented along the load is roughly 1500, i.e. only 25% of the fibres are load-bearing. This justifies our earlier assumption that a disentangled fibre is nearly always replaced by a new load-bearing one. From figure 4*b*, we estimate the maximal force that an individual fibre experiences to be $O(10^{-2})$ N well below the threshold for plastic deformation (10^{-1} N from figure 1). This confirms that the response is elastic at the fibre scale, while macroscopic plastic effects arise mainly owing to network reorganization.

5. DISCUSSION

Synthetic felt embodies the two generic features of biological fibre networks, strain stiffening and unusually high Poisson ratio. Here we have emphasized the geometric basis of these physically observed collective effects by studying synthetic fibrous networks which provide us with the significant advantages of easy visualization and manipulation, while allowing us to separate the influence of geometry and connectivity from molecular effects.

We find that the measured strain stiffening follows directly from the nonlinearity of the single fibre mechanical response, broadly consistent with other recent studies of microscopic polymer networks (Gardel *et al.* 2004; Storm *et al.* 2005), although the qualitative details differ owing to the fact that the underlying microscopic physics in these synthetic fibrous networks is dominated by the quenched curvature that is a result of the processing rather than a consequence of thermal fluctuations as in polymers. A simple geometrically nonlinear model for the fibre accounting for the measured quenched curvature also allows us to quantitatively explain our observations. The unusually high values of the Poisson ratio rely on a more universal property of fibrous materials, since fibres buckle easily under a compressive load and stiffen under tension. Thus, a longitudinal stretch generates substantial transverse compressive strain in our simple unit cell and leads to a large transverse strain at the level of the network. The densification of the network observed by us is therefore a direct consequence of the inability of a fibrous network to sustain compressive loads; indeed, similar results are seen in uniaxial tests with other fibrous materials such as collagen (Roeder *et al.* 2004*b*). High values for the incremental Poisson ratio are expected to arise generically in all these systems as soon as the local stress exceeds a microscopic buckling threshold, *a priori* dependent on the fibre bending stiffness and the typical distance between crosslinks.

More generally, in the context of biological networks in such situations as the cytoskeleton, blood clots and collageneous tissues, our conceptual framework provides a baseline from which the effects of the mechanochemical coupling, growth and kinetic reorganization can be built on. Of the many questions that these more complex biomechanical networks pose, a natural question that our study raises is the role of small stress inhomogeneities and/or anisotropy, generated, for example, by cells embedded in networks, which can dramatically change the macroscopic mechanical properties of tissues. These are probably already used by Nature and most definitely could be exploited in engineering artificial tissues and fibrous materials.

We thank K. Brakke for his assistance in modifying Surface Evolver to help with our preliminary calculations of the response of curved fibres.

APPENDIX A. MULTISCALE APPROACH FOR FIBRE RESPONSE

The linear analysis developed in the paper is valid only if the local angle between the fibre and the force direction is small. Figure 5 shows the typical response for a curvature with two well-separated length-scales characterizing the natural shape of the fibre, with $\kappa_0(s) = \kappa_1(s) + \kappa_2(s) = 40\cos(16\pi s) + 5\cos(2\pi s)$. The force–extension relationship obtained by solving equations (3.2) and (3.3) shows two regimes: initially, small forces stretch out the long wavelength mode, while the short wavelength mode is stretched out for higher forces. The linear approximation of equation (3.2) yields results that disagree with the numerical solution for small forces, as expected.

For fibres with two widely separated length-scales, we may use a multiple scale approach to combine solutions obtained for each individual length-scale. Let $\mathrm{A}(s) = \mathrm{A}_i(s) + \mathrm{A}_2(s)$ be the solution of equation (3.2) with $\kappa_0(s) = \kappa_1(s) + \kappa_2(s)$, where $\kappa_1(s)$ varies rapidly and $\kappa_2(s)$ varies slowly. If θ_1 is the solution corresponding to the rapidly varying curvature, it satisfies the equation

$$-\frac{f}{B}\sin\theta_1 + \frac{\partial^2\theta_1}{\partial s^2} = \frac{\partial\kappa_1}{\partial s}. \qquad (\mathrm{A}\,1)$$

Assuming that $\theta_2 = \theta - \theta_1$ is small, equations (3.3) and (A1) yield

$$-\frac{f}{B}\theta_2\cos\theta_1 + \frac{\partial^2\theta_2}{\partial s^2} = \frac{\partial\kappa_2}{\partial s}. \qquad (\mathrm{A}\,2)$$

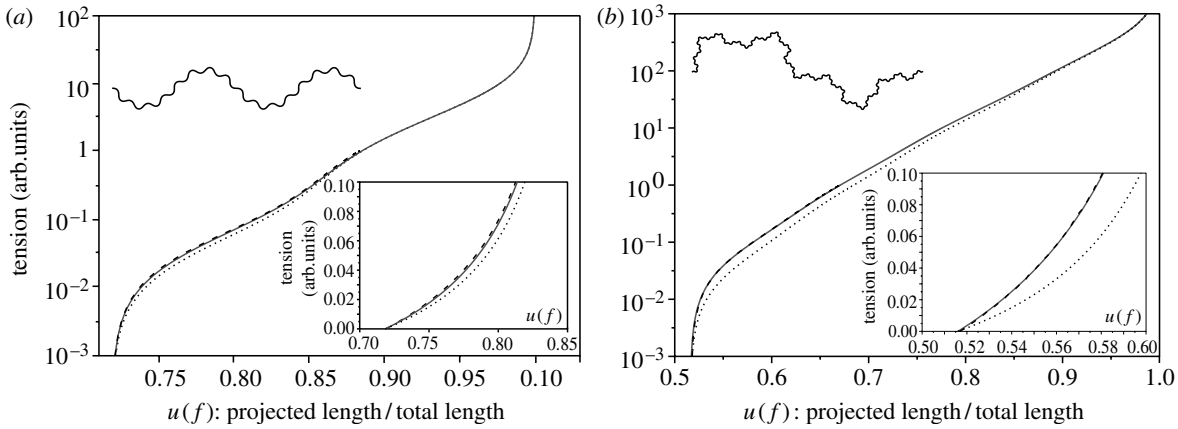

Figure 5. Multiscale approach for fibre response: the dashed line corresponds to the numerical solution of (3.2)–(3.3) and the dotted line approximation (3.3)–(3.4). The solid line is the corrected solution using (A5), (A6) and (A8) for two different shapes (*a*) $\kappa_0(s)=40\cos(16\pi s)+5\cos(2\pi s)$ and (*b*) $\kappa_0(s)=320\cos(128\pi s)+80\cos(32\pi s)+20\cos(8\pi s)+5\cos(2\pi s)$. The Insets show the natural shapes of these filaments and a blow-up of the low force-extension regime.

Integrating this equation over the short wavelength modes yields the approximate equation

$$-\frac{f}{B}u_1(f)\cdot\theta_2+\frac{\partial^2\theta_2}{\partial s^2}=\frac{\partial\kappa_2}{\partial s}, \tag{A 3}$$

with $u_1(f)=\langle\cos(\theta_1(s,f))\rangle_s$, where the angular brackets denote an average over the short wavelength modes. We see that θ_2 satisfies equation (3.2), but with an effective bending stiffness ($B\rightarrow B/u_1$). In figure 4*b*, the solid line is the analytical solution obtained with this approximation and is in excellent agreement with the complete numerical solution. Generalizing this approach to an arbitrary but finite number of modes with well-separated length-scales and small amplitudes, our goal is to derive an approximate solution $\theta(f,s)$ of the equation

$$-\frac{f}{B}\sin(\theta)+\frac{\partial^2\theta}{\partial s^2}=\sum_{i=1}^{N}\frac{\partial\kappa_i(s)}{\partial s}, \tag{A 4}$$

with $\kappa_0=\sum_{i=1}^{N}\kappa_i(s)$, where κ_i is a single length-scale curvature. Defining $\boldsymbol{\Theta}_i(f,s)$ as the solution to

$$-\frac{f}{B}\cdot\boldsymbol{\Theta}_i+\frac{\partial^2\boldsymbol{\Theta}_i}{\partial s^2}=\frac{\partial\kappa_i}{\partial s}, \tag{A 5}$$

and the response function $u_i(f)$ using

$$u_i(f)=\langle\cos(\boldsymbol{\Theta}_i(f,s))\rangle_s, \tag{A 6}$$

allows us to write the solution as

$$\theta(f,s)=\sum_{i=1}^{N}\boldsymbol{\Theta}_i\left(f\cdot\prod_{j=0}^{i-1}u_j(f)\right)\ \text{with}\ u_0(f)=1. \tag{A 7}$$

The resulting force–extension relationship is then given by

$$\begin{aligned}u(f)&\simeq\left\langle\cos\left(\sum_{i=1}^{N}\boldsymbol{\Theta}_i\left(f\cdot\prod_{j=1}^{i-1}u_j(f)\right)\right)\right\rangle_s\\&\simeq\prod_{i=1}^{N}\left\langle\cos\left(\boldsymbol{\Theta}_i\left(f\cdot\prod_{j=1}^{i-1}u_j(f)\right)\right)\right\rangle_s\\&\simeq\prod_{i=1}^{N}u_i\left(f\cdot\prod_{j=0}^{i-1}u_j(f)\right),\end{aligned} \tag{A 8}$$

with $u_0(f)=1$ for an inextensible filament. On the other hand, for a filament with a finite stretching modulus, we use equation (A7) or (A8) and set $u_0(f)=1+f/\Gamma$, where Γ is the stretching modulus of the rod. This completes our approximate multiscale analysis for the response of a single fibre, and thence that of the network.

For monotonically stiffening materials, such as skin and other biological tissues, a well accepted empirical constitutive law (Fung 1993) assumes that the stress is exponential in the strain, which law is consistent with our data for the strain-stiffening felt as well. However, our analysis and experiments show that the underlying microscopic mechanism is the quenched curvature distribution of the individual filaments. This leads to a concatenation of power laws for the stress–strain law which approximates an exponential stress–strain relation well, but is nevertheless qualitatively different.

REFERENCES

Alberts, B., Johnson, A., Lewis, J., Raff, M., Roberts, K. & Walter, P. 2002 *Molecular Biology of the Cell*, 2nd edn. New York, NY: Garland Science.

Becker, N., Oroudjev, E., Mutz, S., Cleveland, J. P., Hansma, P. K., Hayashi, C. Y., Makarov, D. E. & Hansma, H. G. 2003 Molecular nanosprings in spider capture-silk threads. *Nat. Mater.* **2**, 278–283. (doi:10.1038/nmat858)

Blatz, P. J., Chu, B. M. & Wayland, H. 1969 On the mechanical behavior of elastic animal tissue. *Trans. Soc. Rheol.* **13**, 83–102. (doi:10.1122/1.549157)

Chandran, P. L. & Barocas, V. H. 2006 *J. Biomech. Eng.* **128**, 259–270. (doi:10.1115/1.2165699)

Chawla, K. K. 1998 *Fibrous materials*. Cambridge, UK: Cambridge University Press.

Cluzel, P. A., Lebrun, A., Heller, C., Lavery, R., Viovy, J. L., Chatenay, D. & Caron, F. 1996 DNA: an extensible molecule. *Science* **271**, 792–794.

Fernandez, P., Pullarkat, P. A. & Ott, A. 2006 A master relation defines the nonlinear viscoelasticity of single fibroblasts. *Biophys. J.* **90**, 3796.

Flory, P. J. 1959 *Principles of polymer chemistry*. Ithaca, NY: Cornell.

Fudge, D. S., Gardner, K. H., Forsyth, V. T., Riekel, C. & Gosline, J. M. 2003 The mechanical properties of hydrated intermediate filaments: insights from hagfish gland thread cells. *Biophys. J.* **85**, 2015–2017.

Fung, Y. C. 1993 *Biomechanics: mechanical properties of living tissues*. Berlin, Germany: Springer.

Gardel, M. L., Shin, J. H., MacKintosh, F. C., Mahadevan, L., Matsudaira, P. & Weitz, D. A. 2004 Elastic behavior of cross-linked and bundled actin networks. *Science* **304**, 1301–1305. (doi:10.1126/science.1095087)

Head, D. A., Levine, A. J. & MacKintosh, F. C. 2003 Deformation of cross-linked semiflexible polymer networks. *Phys. Rev. Lett.* **91**, 108102. (doi:10.1103/PhysRevLett.91.108102)

Hearle, J. W. S., Grosberg, P. & Backer, S. 1969 *Structural mechanics of fibers, yarns, and fabrics*. New York, NY: Wiley-Interscience.

Heussinger, C. & Frey, E. 2006 Stiff polymers, foams and fiber networks. *Phys. Rev. Lett.* **96**, 017802. (doi:10.1103/PhysRevLett.96.017802)

Janmey, P. A., Amis, E. J. & Ferry, J. D. 1983 Rheology of fibrin clots. VI. Stress relaxation, creep, and differential dynamic modulus of fine clots in large shearing deformations. *J. Rheol.* **27**, 135–153. (doi:10.1122/1.549722)

Layton, B. E. & Sastry, A. M. 2004 A mechanical model for collagen fibril load sharing in the peripheral nerve of diabetic and non-diabetic rats. *J. Biomech. Eng.* **126**, 803–814. (doi:10.1115/1.1824118)

Lee, M. E. M. & Ockendon, H. 2005 A continuum model for entangled fibres. *J. Appl. Math.* **16**, 145–160. (doi:10.1017/S0956792505006170)

Love, A. E. H. 1944 *A treatise on the mathematical theory of elasticity*. New York, NY: Dover.

MacKintosh, F. C., Käs, J. & Janmey, P. A. 1995 Elasticity of semiflexible biopolymer networks. *Phys. Rev. Lett.* **75**, 4425–4428. (doi:10.1103/PhysRevLett.75.4425)

Marko, J. F. & Siggia, E. D. 1995 Stretching DNA. *Macromolecules* **28**, 8759–8770. (doi:10.1021/ma00130a008)

Maxwell, J. C. 1864 On the calculation of the equilibrium and stiffness of frames. *Phil. Mag.* **27**, 294–299.

Onck, P. R., Koeman, T., van Dillen, T. & van der Giessen, E. 2005 Alternative explanation of stiffening in cross-linked semiflexible networks. *Phys. Rev. Lett.* **95**, 178102. (doi:10.1103/PhysRevLett.95.178102)

Roeder, B. A., Kokini, K., Sturgis, J. E., Robinson, J. P. & Voytik-Harbin, S. L. 2004*a* Tensile mechanical properties of three-dimensional type I collagen extracellular matrices with varied microstructure. *J. Biomech. Eng.* **124**, 214–222. (doi:10.1115/1.1449904)

Roeder, B. A., Kokini, K., Robinson, J. P. & Voytik-Harbin, S. L. 2004*b* Local, three-dimensional strain measurements within largely deformed extracellular matrix constructs. *J. Biomech. Eng.* **126**, 699–708. (doi:10.1115/1.1824127)

Ryan, E. A., Mockros, L. F., Weisel, J. W. & Lorand, L. 1999 Structural origins of fibrin clot rheology. *Biophys. J.* **77**, 2813–2826.

Sacks, M. S. 2000 Biaxial mechanical evaluation of planar biological materials. *J. Elasticity* **61**, 199–246. (doi:10.1023/A:1010917028671)

Shadwick, R. E. 1999 Mechanical design in arteries. *J. Exp. Biol.* **202**, 3305–3313.

Smith, S. B., Cui, Y. & Bustamante, C. 1996 Overstretching B-DNA: the elastic response of individual double-stranded and single-stranded DNA molecules. *Science* **271**, 795–799.

Storm, C., Pastore, J. J., MacKintosh, F. C., Lubensky, T. C. & Janmey, P. A. 2005 Nonlinear elasticity in biological gels. *Nature* **435**, 191–195. (doi:10.1038/nature03521)

Treloar, A. 1972 *Physics of rubber elasticity*, 3rd edn. Oxford, UK: Claredon Press.

Vincent, J. F. V. 1990 *Structural biomaterials*. New Jersey, NJ: Princeton University Press.

Weisel, J. W. 2004 The mechanical properties of fibrin for basic scientists and clinicians. *Biophys. Chem.* **112**, 267–276. (doi:10.1016/j.bpc.2004.07.029)